Phonon predictions with E(3)-equivariant graph neural networks

Shiang Fang*
Department of Physics
Massachusetts Institute of Technology
Cambridge, MA, USA
shiangf@mit.edu

Mario Geiger*
Department of Electrical Engineering
and Computer Science,
Massachusetts Institute of Technology
Cambridge, MA, USA
geiger.mario@gmail.com

Joseph G. Checkelsky
Department of Physics
Massachusetts Institute of Technology
Cambridge, MA, USA
checkelsky@mit.edu

Tess Smidt
Department of Electrical Engineering
and Computer Science,
Massachusetts Institute of Technology
Cambridge, MA, USA
tsmidt@mit.edu

Abstract

We present an equivariant neural network for predicting the phonon modes of the periodic crystals and molecules by evaluating the second derivative Hessian matrices of the energy model, which are first trained with the energy and force data. Such efficient Hessian prediction enables us to predict the phonon dispersion and the density of states for inorganic crystal material and can be fine-tuned with additional dataset. For molecules, we also derive the symmetry constraints for infrared/Raman active modes by analyzing the phonon mode irreducible representations. Our training paradigm further shows using Hessian as a new type of higher-order training data to improve the energy models beyond the lower-order energy and force data.

1 Introduction

The vibration phonon modes of the atoms in a structure play a crucial role in determining the material properties such as the thermal, and transport characteristics in various applications [20, 24, 23, 37, 25, 17, 29]. The symmetry characteristics of these modes determine their behavior when they are studied using infrared/Raman spectroscopy [1]. In solids, the unstable phonon modes at negative (or imaginary) energy also provide intuition for the potential symmetry breaking of the crystal structure, as in the perovskite structures [34]. In high-throughput material search and AI-guided design, it is therefore crucial to have an efficient tool to predict the phonon properties given an atomic structure. The advances in machine learning and deep neural networks have inspired significant progress in parametrizing atomic potentials using physics-informed equivariant neural network models [26, 3, 4]. In this work, we utilize such symmetry-aware E(3)-equivariant graph neural network models [14, 13] to achieve efficient and accurate phonon predictions by direct computations of the Hessian matrices. Our training paradigm further generalizes the training data types by including the Hessian data as a higher-order extension beyond the energy and force data at the zeroth and first order respectively.

*Equal Contribution. Order is random.

37th Conference on Neural Information Processing Systems (NeurIPS 2023).

1.1 Main contributions

- We applied a second derivative method to determine the phonon dynamical matrices in periodic crystals. For these calculations, we utilize energy models pre-trained on the Universal-IAP dataset [8]. As energy models, we employ the architectures of NequIP [4] and MACE [3]. To ensure precise evaluations of the dynamical matrices in periodic crystals, we also devised an extended graph construction technique.
- Besides the phonon Hessian predictions, we also demonstrated using the Hessian data (evaluated from DFT/DFPT [16]) as additional second-order training data beyond energy and forces to further improve the energy models.
- For molecular cases, we implement tools to extract the phonon mode symmetry irreducible representations [7] and the active modes for infrared/Raman experimental probes under symmetry selection rules [1].

1.2 Related work

Previously, phonon predictions were shown to be derived from atomic potential models by evaluating the forces for the slightly displaced atomic patterns near their equilibrium positions [8, 28]. These methods require choices of supercell geometries and the enumerations of the independent displacement pattern subject to the crystallographic symmetry constraints, and the finite-difference approximation for getting numerical Hessians (frozen phonon method). Due to the supercell geometries adopted, the phonon bands are folded and one has to apply band structure unfolding to get the conventional phonon spectrum [38, 40, 39]. On the other hand, the virtual node method VGNN [27] targets the dynamical matrix prediction directly without generating an energy model from the training process.

2 Phonax: equivariant neural networks for phonon predictions

2.1 Formulation for vibrational phonon modes

The equation of motion for the atoms vibrating around their equilibrium locations in the crystal structure is governed by the dynamical matrix [20, 24]

$$D_{\alpha\beta}(ij,\vec{q}) = \frac{1}{\sqrt{m_i m_j}} \sum_a \frac{\partial^2 E}{\partial(\vec{x}_{0i})_\alpha \partial(\vec{x}_{aj})_\beta} e^{i\vec{q}\cdot(\vec{x}_{aj}-\vec{x}_{0i})} \tag{1}$$

at crystal momentum $\vec{q}$ with unit cell index a, atomic basis indices i, j, and $\alpha, \beta = x, y, z$. The phonon eigenvalue equation is given by

$$\sum_{j\beta} D_{\alpha\beta}(ij,\vec{q}) e^n_\beta(j,\vec{q}) = [\omega^n(\vec{q})]^2 e^n_\alpha(i,\vec{q}) \tag{2}$$

for the n-th phonon modes with energy $\omega^n(\vec{q})$ and normal mode wavefunction $e^n_\beta(j,\vec{q})$. The molecular case is simplified with $\vec{q} = 0$ without crystal momentum. For the periodic crystal case at momentum $\vec{q}$, the symmetry little group dictates the types of symmetry irreducible representations of the phonon modes and energy level degeneracy, which leads to the symmetry selection rules for experimental infrared/Raman spectroscopy [1]. For the polar crystals, the atomic vibrations further induce electric dipole moments that can interact via long-range dipole-dipole interactions [16]. A rigorous treatment requires additional inputs for the Born effective charges and the dielectric constant tensor, and the Ewald sum for the long-range interaction is shown to give rise to singular contributions near $\vec{q} \to 0$. This non-analytical term correction and the resulting phonon band discontinuity near Γ are also known as the LO-TO splitting [33]. In our work here, we neglect such corrections and leave these dipole-dipole corrections to future work.

2.2 Model Architecture

The equivariant neural network atomic potential models are symmetry-aware and efficient in predicting accurate atomic energy and force interactions. In our work, we have used NequIP [4] and MACE [3] models as our energy foundation models. To evaluate the phonon dynamical matrix, one

needs to evaluate the second derivatives with respect to the pairs of atomic coordinates in the structure as appear in the dynamical matrix. For the computational graph, however, one has to generalize the conventional periodic crystal graph which retains only the coordinates within the center unit cell (which leads to the single unit cell periodicity and $\vec{q} = 0$ constraint). In a message-passing neural network architecture as shown in Fig. 1b, r_c sets the cutoff for the information flow in one iteration of the message-passing (spacing for one unit cell in this 1D chain example). With n_m steps of message-passing convolutions ($n_m = 2$), one has an enlarged cutoff radius $n_m r_c$ for the information flow. We constructed the extended graph to capture these by including all the atomic sites from the surrounding unit cells within such receptive fields of the center unit cell, see Fig. 1b for the illustration. We implemented these within JAX framework [6], using e3nn-jax [12, 13], jraph [15], Haiku [18], JAX-MD [36] and MACE-JAX [2, 3] libraries. In the following results, we focus on training using the NequIP model.

3 Results

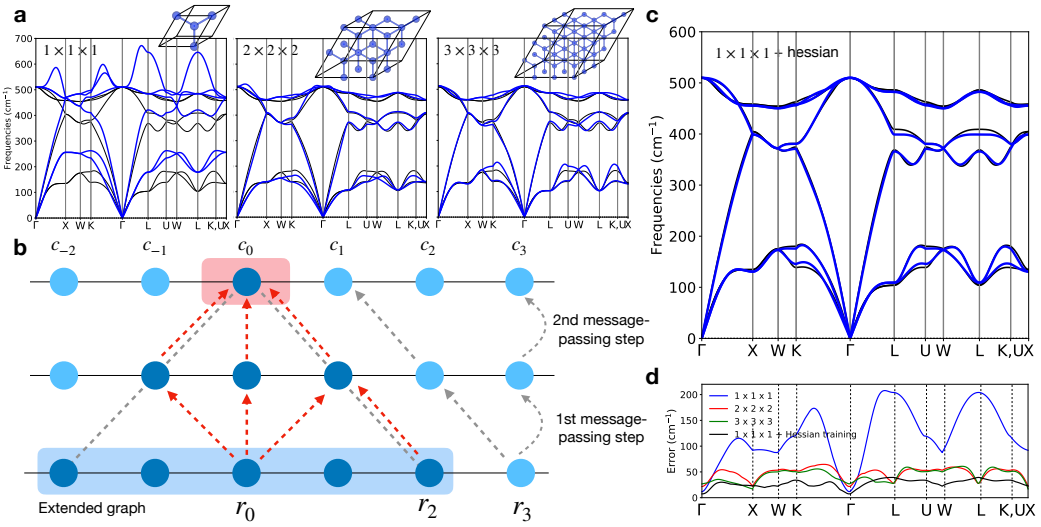

Figure 1: **Phonon prediction and training:** (a) Si crystal phonon predictions (mp-149) in blue using the NequIP models trained with $1\times1\times1$, $2\times2\times2$ and $3\times3\times3$ supercell energy/force data, which has 2, 16, 54 atoms respectively. The ground truth DFT phonon bands are shown in black. (b) The illustration for the information flow with a 1D chain. Within each iteration step of the message-passing graph neural network, c_i site gathers messages from $c_{i\pm1}$ sites. With a total $n_m = 2$ iterations, the center unit c_0 incorporates features from c_i with $-2 \leq i \leq 2$. These sites constitute the extended graph for Hessian evaluation. Within this model, $\partial^2 E/\partial r_0 \partial r_j = 0$ for $|j| > 2$. (c) The energy model is trained with $1\times1\times1$ and the Hessian data. The phonon prediction is significantly better than using only $1\times1\times1$ data shown in a. (d) The error analysis in the momentum space for phonon predictions in a and c. At each $\vec{q}$, these errors are computed from the matrix norm for the errors in the predicted dynamical matrix. The model trained with additional Hessian data (black) achieves the lowest error overall.

3.1 Phonon Predictions for Crystals with a Periodic Lattice

In Fig. 1, we first show the predicted phonon spectrum for the silicon atom in the diamond structure (mp-149). We have trained the energy model using energy / force data from various sizes of supercells in Fig. 1a, and the phonon predictions are more accurate for larger supercells to allow independent degrees of freedom. Next, we augmented the smallest $1\times1\times1$ force data with Hessian data. Interestingly, these predictions outperformed those from the model trained on the largest $3\times3\times3$ supercell. Please see Figs. 1c and 1d for the predicted spectrum and error analysis. It is worth noting here that there are three $E = 0$ modes at Γ point. These zero modes appear due to the crystal energy invariance under a uniform translation of atomic positions. In our modeling framework, those

zero modes are built-in as the inductive bias. Without strictly enforcing this symmetry numerically, correction terms would be needed to restore these zero modes, as per the acoustic phonon sum rule.

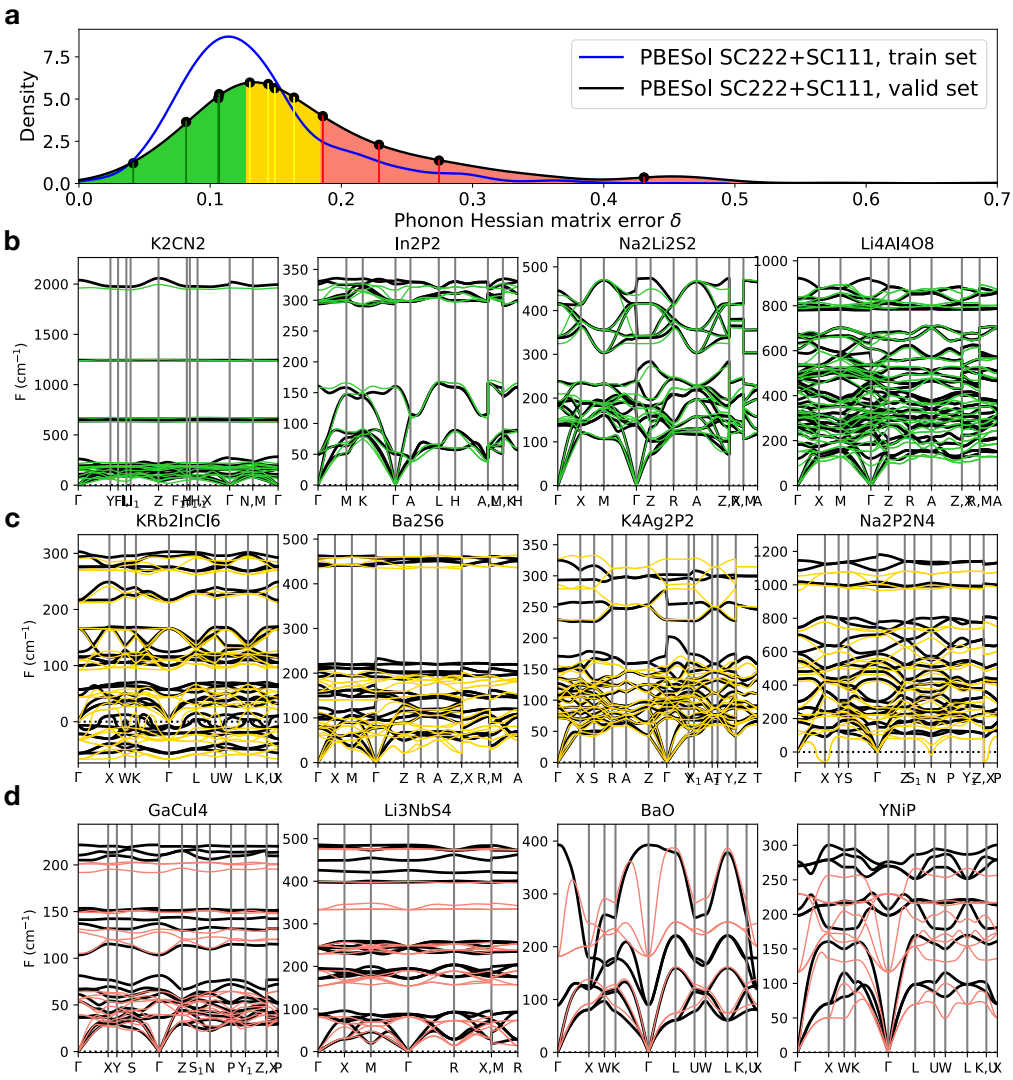

Figure 2: **Phonon prediction for the periodic crystals and the error analysis** (a) The distribution for the phonon predictions error metric of the periodic crystals with the PBESol model evaluated for the train and valid datasets. The crystals are grouped into three tertiles depending on the error metric (shaded areas for the valid dataset). Crystal examples are drawn randomly from the (b) first tertile (c) second tertile (d) third tertile groups in the prediction accuracy. The predicted phonon bands are colored green, yellow, and red respectively with the ground truth DFT results in black for the comparison.

Having verified our phonon prediction method above, we used the universal-IAP dataset [8] to train the general-purpose energy model based on NequIP architecture, with energy / force data from the Materials Project [19]. To remove the data with extremely large atomic forces and limit our training near the equilibrium configurations, we impose a force cutoff 5 eV/Å to filter the dataset. We allocated 3% of the crystal structures as the validation dataset, using the remaining 97% for training. While the universalIAP calculations were done with the PBE approximation for the exchange-correlation functional [30], the phonon database [32] with the Materials Project was computed with PBEsol functional [31]. To correct the model due to the exchange-correlation functional, we carried out additional VASP DFT calculations [22, 21, 5] with PBEsol to get the energy and force data for the supercell structures with atomic positions randomly perturbed (Gaussian noise ≈ 0.1Å, see SI for more details). With this dataset, we train our energy model and the predicted phonon results show better agreement. In Fig. 2, we show the phonon predictions and error analysis for crystals in the phonon database.

3.2 Training and data augmentation with molecular Hessians

As in the periodic crystal cases, the molecular Hessians can be used to derive the vibrational modes in the molecules. One can further derive the symmetry properties of these normal modes, and the associated IR/Raman active mode selection rules, which have implications on the experimental identifications (see SI for more details.). Here we use the molecular Hessian data as the additional training data to improve the energy model. To generate the training dataset, we used the ethanol molecular configurations in the CCSD dataset [10] (drawn from MD simulations, see SI for the dataset construction) and computed the energy, atomic forces, and the full hessian with VASP DFT. In Fig. 3a, we showed how the force generalization errors are affected by a single configuration training, using only the force data, compared with the training using force and Hessian data. The force validation datasets are constructed by adding positional Gaussian noise at various strength to the training ethanol configuration. The training curve shows how the generalization errors are much reduced with Hessian training data. It remains an interesting open question to see if such an energy model would be more stable under MD simulations [11], as the local stability is controlled by the second derivative Hessians.

Next in Fig. 3b, we show the training curve comparisons with and without using the hessian data for the force MAE in the valid dataset, with varying number of molecular configurations used. Although the force MAE improves when hessian data is included, it does not yet lead to a stronger scaling from the slope. The shifted curve suggests an effective 5 times the number of force configurations in this training case with ethanol. Physically, the hessian provides a more complete prescription of the energy landscape around a given atomic structure compared to the force-only training, and therefore effectively augments the training configurations.

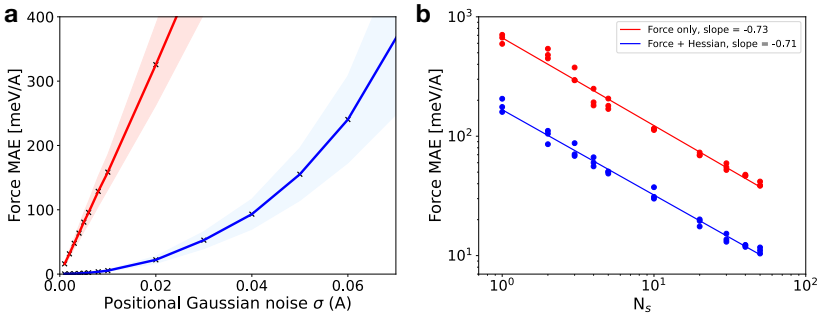

Figure 3: **Molecules and Hessians:** (a) The evaluation for energy model trained with a single ethanol configuration, using only the force data, or force+Hessian. The force MAE is computed with slightly perturbed molecular configurations with positional Gaussian noise σ from 0.001Å to 0.07Å from the trained configuration. 100 trainings (seeds + random samples) were used at each σ with the std for force MAE represented by the shaded area. With Hessian data training, force MAE is strongly suppressed around the molecular configuration. (b) The training curve for the scaling of the prediction error with the number of training configurations.

4 Conclusions

In this work, we predict the phonon dynamical matrices by deriving the second-derivative Hessians of the energy model parametrized by E(3)-equivariant graph neural networks. We have accurately forecasted the vibrational characteristics of both periodic crystals and molecules. Additionally, we have shown that incorporating Hessian data into our dataset enhances the training of our energy model. Beyond the models we have pre-trained, one can further fine-tune the model with additional energy/force data for a specific family of materials, or more refined ab initio calculations to achieve more accurate predictions.

5 Broader Impact

We consider here the two aspects of our work. The first one is the efficient prediction of the phonon modes and their properties. In the high-throughput search for the materials, this is a crucial step to screen or evaluate the material candidates in the applications. Our pre-trained general-purpose models enable such predictions for general element types in the periodic table and crystal structures. On the other hand, the vibrational phonon modes also inform the energetic and mechanical properties of the materials. Despite being second-derivative data, phonon properties connect more directly to the realistic observations compared to the first-order force data. Our phonon prediction model would allow the training to use experimental or simulated phonon data to further improve the underlying energy model.

6 Acknowledgments and Disclosure of Funding

This work was supported by the DOE ICDI grant DE-SC0022215 and the Gordon and Betty Moore Foundation EPiQS Initiative, Grant No. GBMF9070. The authors acknowledge the MIT SuperCloud [35] and Lincoln Laboratory Supercomputing Center for providing HPC resources that have contributed to the results reported herein.

7 Supplementary Information

7.1 Dataset generated: Phonon predictions with PBEsol energy/force training data

The universal-IAP data we used to pre-train the energy model was computed with DFT calculations using the PBE exchange-correlational functional [30]. However, the phonon database [32] (used in the Materials Project) was derived from DFPT calculations based on DFT calculations with PBEsol exchange-correlational functional [31]. The differences between the exchange-correlational functionals used lead to different DFT predictions given an atomic structure. The main differences include the following: the equilibrium stable structure, and the energy/force predictions for a structure. The equilibrium structure implies the lattice constants of the cell vectors and the atomic positions in a unit. Mixing the two different DFT data would reduce the prediction accuracy. Therefore, we train another energy model based on these PBEsol energy / force data besides the general-purpose energy model trained with PBE data. [One can further explore the ideas to fine-tune the pre-trained PBE model with this additional dataset.]

To generate such PBEsol fine-tuning data, we focus on the ~ 1.5k periodic crystals used in the phonon database [32]. The data generated includes several types and we have adopted the same train-test data split in phonon DOS prediction work [9]. First, we consider the unperturbed crystal structure and employed DFT to compute the energy and force data of these structures with PBEsol [31]. Note that while the original phonon database was computed with Abinit DFT code, VASP DFT calculations were carried out here. The results are consistent in that these structures are near equilibrium with small residual forces and stress within the crystals. Besides the equilibrium structures, we also augment the data generation with perturbed periodic crystal structures. We retain the same $1\times1\times1$ unit cell periodicity, and generate perturbed structures with Gaussian noise added to the atomic site positions Two types of perturbations are generated which depend on whether Gaussian noises were also added to the unit cell vectors or not.

	Cell noise	Positional noise	Train	Valid
Equilibrium structures	N	N	1	-
$1 \times 1 \times 1$ structures	N	Y	2	1
$1 \times 1 \times 1$ structures'	Y	Y	2	1
$2 \times 2 \times 2$ structures	N	Y	2	1
$2 \times 2 \times 2$ structures'	Y	Y	2	1

Table 1: PBEsol augmentation energy and force data types. The values in the train/valid indicate the number of randomly perturbed samples given a structure. (equilibrium structures are without the Gaussian noise perturbations.)

As shown in the main text Fig 1, the phonon predictions can be improved by using the energy / force data from enlarged supercell structures which can unfold the atomic pair interactions. To derive such data augmentation, we repeat the calculations with enlarged $2\times2\times2$ unit cell periodicity and add perturbations. The Gaussian noise added to the atomic positions has a $\sigma = 0.1$Å, while the Gaussian noise added to the cell vectors (supercell) has a $\sigma = 0.05$Å.

In Table 1, we summarize the types of data generated for PBEsol model fine-tuning. We used this dataset to train a NequIP energy model and derive the phonon predictions for the crsytals in the valid dataset (about 330 crystals). In Fig. 2 a, we plot the Hessian error metric, which is defined by the ratio between the matrix norms for the errors in the dynamical matrix prediction and the ground truth dynamical matrix, averaged over the BZ k point sampling. Based on this error analysis, we group the crystals from the valid dataset into three tertiles, and draw random examples for deriving their phonon spectrum shown in Fig. 2 b-d.

7.2 Molecular Hessian data generation and training procedure

In this section, we describe the molecular Hessian database generation with DFT calculations. Intuitively, the Hessian matrices describe the force constants of an atomic structure, a 3×3 force constant matrix for each atomic pair (or within a single atomic site). To generate this molecular Hessian database, we adopted the molecular configurations from the CCSD database [10] which includes five types of molecules, ethanol, malonaldehyde, benzene, toluene, and aspirin. [In the original work to generate this CCSD database [10], the goal was to build a molecular energy/force database beyond the DFT-level approximations and achieve more accurate quantum-chemistry level predictions. Despite being more advanced and accurate compared to the conventional DFT calculations, the molecular configurations were derived from MD simulations at the DFT level, with the CCSD corrections calculated on top of molecular configurations sampled from the MD trajectories.] In our Hessian database generation, we took the molecular geometric configurations in this CCSD database, and recalculated the energy and force data using the VASP DFT code [22, 21], using the same train-test data split. The electronic ground states were converged with an energy cutoff 500 eV, and PBE exchange-correlation functional with PAW formalism, for these molecules enclosed within a $10!\times!10!\times!10$ (in Å) large supercell to reduce interactions between periodic structure images. On top of the converged ground state calculations, the Hessian matrices were then derived with the density functional perturbation theory (DFPT) approach that computes the second-derivatives of the total molecular energy with respect to the atomic positions within the molecule (rather than the finite-difference method). The calculation results were then post-processed by the Phonopy python library [38, 40, 39], to extract the Hessian matrices. To be consistent with the Hessian data derived, we also extract the molecular energy and atomic force data from the DFT calculations, such that they all describe the same energy landscape of the molecular configuration with the data as different orders of derivatives.

For the data generated given a molecule with N atoms, the force data can be stored in a $N \times 3$ matrix, while the Hessian data requires a $N \times N \times 3 \times 3$ tensor for the storage. The geometric symmetries of the atomic structure would further simplify the Hessian matrices by imposing further constraints which reduce the independent coupling parameters. For example, the translational invariance of the molecular energy leads to the acoustic sum rule and zero energy modes in the spectrum. In our Hessian database construction, we do not impose the acoustic sum rule of the numerical Hessian

matrices. Instead, this symmetry constraint is baked into our equivariant neural network as an inductive bias.

The training data is then generated by selecting the Hessian matrix element from randomly chosen pairs of atomic coordinates, projected in randomized directions to retain rotational equivariance. In the training, second derivative Hessians were only evaluated with the selected atomic site pairs and associated projected directions, without evaluating the full molecular Hessian which could be time consuming. Besides the training signal (gradient) from Hessian data, we also mix it with the weighted training signal from comparing force data.

7.3 Molecular Hessians: symmetry analysis for infrared/Raman-active modes

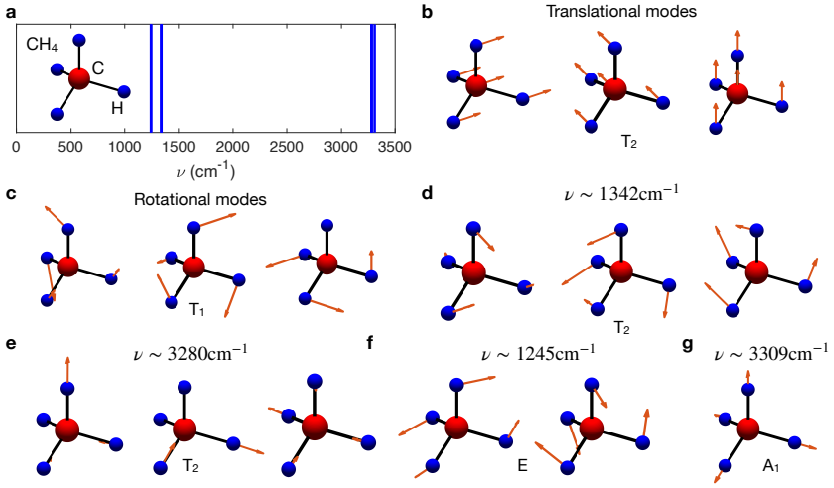

Figure 4: **CH_4 molecule vibrational modes and the symmetry analysis** (a) We have derived the vibrational spectrum of the CH_4 molecule which has a T_d point group symmetry. First, we identify and remove the zero energy modes from the pure (b) translational modes (with T_2 symmetry representation) and (c) rotational modes (with T_1 symmetry representation). The rest of the predicted modes are at (d) 1342 cm^{-1} T_2 mode (e) 3280 cm^{-1} T_2 mode (f) 1245 cm^{-1} E mode (g) 3309 cm^{-1} A_1 mode

In this section, we provide further discussions on the symmetry analysis for the molecular vibrational modes and conditions for the infrared / Raman-active modes from the molecular point group symmetry [1]. Given a molecular structure at equilibrium, the energy is invariant under the real space translations and the rotations with respect to the molecule center of mass point. This energy invariance leads to 6 zero modes in the vibrational spectrum: three translational modes and three rotational modes. In our construction, we use uniform translations in x, y, z directions respectively to define the translational modes. For the rotational modes, we define them as the infinitesimal rotations with respect to the x, y, z axes for the coordinate frame defined at the molecular center of mass (therefore the vector cross-product of the atomic positional vector and the rotation axis). In terms of symmetry content, the three translation modes contain the vector-like irreducible representation(s) under the point group symmetry of the molecule (i.e. as x, y, z basis functions in the point group character table). On the other hand, the three rotational modes transform as the anti-symmetric tensors or the $\mathcal{R}_x, \mathcal{R}_y, \mathcal{R}_z$ objects in the point group character table.

To filter out these modes, we define the projectors based on the translational and rotational modes described above. Once such a projector is constructed, one can evaluate the projected eigenstate norm for the vibrational modes, and remove the 6 states with the largest projections (numerically near the zero energies from the translational and rotational symmetries). We are then left with the non-trivial vibrational phonon modes of the molecules generally at non-zero energies. To extract specific symbols of these symmetry irreducible representation (irrep) for the molecular point group symmetry and the associated vibrational normal modes, we utilize the functions in the posym Python library [7] to analyze the molecular structure point group and the normal mode symmetries.

From the point group theories, it has been shown that the infrared and Raman activities in the experimental probes are related to the symmetry selection rules involving these irreducible symmetry representations of the vibrational modes [1]. For the infrared probes, the coupling Hamiltonian to the optical excitations involves terms that transform as vectors (specifically, the electric dipole moments). To have a non-zero matrix element in the infrared optical excitations, the phonon modes have to contain the vector symmetry representations as well. Therefore, the infrared-active phonon modes are the same as those identified in the translational modes above.

For the Raman-active modes, the symmetry analysis is slightly more involved. In the point group symmetry analysis [1], the Raman transition process involves perturbations that transform as symmetric rank-2 tensors. To derive the Raman-active mode irreps, we first evaluate the rank-2 tensor irreps and then remove the anti-symmetric components. The full rank-2 tensor part can be obtained from the product of two vector irrep(s) as derived from the translational modes above, while the rotational modes derived above contain the same symmetry content as the anti-symmetric. With these, we can derive the symmetry content of the Raman-active mode by subtracting anti-symmetric irrep(s) from the vector product irrep(s), within the posym library framework [7].

As a concrete example, we consider a CH_4 molecule here and its vibrational modes as shown in Fig. 4. A CH_4 molecule has a T_d point group symmetry. We first pre-trained an energy model using NequIP by using only the training data containing H/C/N/O/F elements from the universal IAP dataset [8], then derived the molecular Hessians to obtain the vibrational spectrum and normal modes. With the symmetry selection rules described above, IR active modes are with the T_2 symmetry irreps, while the Raman active modes can be of A_1, E, or T_2 symmetry irreps.

References

[1] *Group Theory*. Springer Berlin Heidelberg, 2008.

[2] Ilyes Batatia, Simon Batzner, Dávid Péter Kovács, Albert Musaelian, Gregor N. C. Simm, Ralf Drautz, Christoph Ortner, Boris Kozinsky, and Gábor Csányi. The design space of e(3)-equivariant atom-centered interatomic potentials, 2022.

[3] Ilyes Batatia, Dávid Péter Kovács, Gregor N. C. Simm, Christoph Ortner, and Gábor Csányi. Mace: Higher order equivariant message passing neural networks for fast and accurate force fields, 2022.

[4] Simon Batzner, Albert Musaelian, Lixin Sun, Mario Geiger, Jonathan P. Mailoa, Mordechai Kornbluth, Nicola Molinari, Tess E. Smidt, and Boris Kozinsky. E(3)-equivariant graph neural networks for data-efficient and accurate interatomic potentials. *Nature Communications*, 13(1):2453, 2022.

[5] P. E. Blöchl. Projector augmented-wave method. *Phys. Rev. B*, 50:17953, Dec 1994.

[6] James Bradbury, Roy Frostig, Peter Hawkins, Matthew James Johnson, Chris Leary, Dougal Maclaurin, George Necula, Adam Paszke, Jake VanderPlas, Skye Wanderman-Milne, and Qiao Zhang. JAX: composable transformations of Python+NumPy programs, 2018.

[7] Abel Carreras. Posym: A python library to analyze the symmetry of theoretical chemistry objects, Oct 2022.

[8] Chi Chen and Shyue Ping Ong. A universal graph deep learning interatomic potential for the periodic table. *Nature Computational Science*, 2(11):718–728, 2022.

[9] Zhantao Chen, Nina Andrejevic, Tess Smidt, Zhiwei Ding, Qian Xu, Yen-Ting Chi, Quynh T. Nguyen, Ahmet Alatas, Jing Kong, and Mingda Li. Direct prediction of phonon density of states with euclidean neural networks. *Advanced Science*, 8(12), March 2021.

[10] Stefan Chmiela, Huziel E. Sauceda, Klaus-Robert Müller, and Alexandre Tkatchenko. Towards exact molecular dynamics simulations with machine-learned force fields. *Nature Communications*, 9(1):3887, 2018.

[11] Xiang Fu, Zhenghao Wu, Wujie Wang, Tian Xie, Sinan Keten, Rafael Gomez-Bombarelli, and Tommi Jaakkola. Forces are not enough: Benchmark and critical evaluation for machine learning force fields with molecular simulations. *TMLR*, 2022.

[12] Mario Geiger, Ameya Daigavane, Song Kim, and Kiarash Jamali. e3nn/e3nn-jax repository on github, 2023.

[13] Mario Geiger and Tess Smidt. e3nn: Euclidean neural networks, 2022.

[14] Mario Geiger, Tess Smidt, Alby M., Benjamin Kurt Miller, Wouter Boomsma, Bradley Dice, Kostiantyn Lapchevskyi, Maurice Weiler, Michał Tyszkiewicz, Simon Batzner, Dylan Madisetti, Martin Uhrin, Jes Frellsen, Nuri Jung, Sophia Sanborn, Mingjian Wen, Josh Rackers, Marcel Rød, and Michael Bailey. Euclidean neural networks: e3nn, April 2022.

[15] Jonathan Godwin*, Thomas Keck*, Peter Battaglia, Victor Bapst, Thomas Kipf, Yujia Li, Kimberly Stachenfeld, Petar Veličković, and Alvaro Sanchez-Gonzalez. Jraph: A library for graph neural networks in jax., 2020.

[16] Xavier Gonze and Changyol Lee. Dynamical matrices, born effective charges, dielectric permittivity tensors, and interatomic force constants from density-functional perturbation theory. *Phys. Rev. B*, 55:10355–10368, Apr 1997.

[17] Kiarash Gordiz, Sokseiha Muy, Wolfgang G. Zeier, Yang Shao-Horn, and Asegun Henry. Enhancement of ion diffusion by targeted phonon excitation. *Cell Reports Physical Science*, 2(5):100431, 2021.

[18] Tom Hennigan, Trevor Cai, Tamara Norman, Lena Martens, and Igor Babuschkin. Haiku: Sonnet for JAX, 2020.

[19] Anubhav Jain, Shyue Ping Ong, Geoffroy Hautier, Wei Chen, William Davidson Richards, Stephen Dacek, Shreyas Cholia, Dan Gunter, David Skinner, Gerbrand Ceder, and Kristin A. Persson. Commentary: The materials project: A materials genome approach to accelerating materials innovation. *APL Materials*, 1(1), July 2013.

[20] C. Kittel, P. McEuen, and John Wiley & Sons. *Introduction to Solid State Physics*. John Wiley & Sons, 2015.

[21] G. Kresse and J. Furthmüller. Efficiency of ab-initio total energy calculations for metals and semiconductors using a plane-wave basis set. *Comput. Mater. Sci.*, 6(1):15, 1996.

[22] G. Kresse and J. Furthmüller. Efficient iterative schemes for ab initio total-energy calculations using a plane-wave basis set. *Phys. Rev. B*, 54:11169, Oct 1996.

[23] Xiyang Li, Peng-Fei Liu, Enyue Zhao, Zhigang Zhang, Tatiana Guidi, Manh Duc Le, Maxim Avdeev, Kazutaka Ikeda, Toshiya Otomo, Maiko Kofu, Kenji Nakajima, Jie Chen, Lunhua He, Yang Ren, Xun-Li Wang, Bao-Tian Wang, Zhifeng Ren, Huaizhou Zhao, and Fangwei Wang. Ultralow thermal conductivity from transverse acoustic phonon suppression in distorted crystalline alpha-mgagsb. *Nature Communications*, 11(1):942, 2020.

[24] Michael P. Marder. *Condensed Matter Physics*. Wiley, October 2010.

[25] Corey Melnick and Massoud Kaviany. Phonovoltaic. i. harvesting hot optical phonons in a nanoscale p-n junction. *Phys. Rev. B*, 93:094302, Mar 2016.

[26] Albert Musaelian, Simon Batzner, Anders Johansson, Lixin Sun, Cameron J. Owen, Mordechai Kornbluth, and Boris Kozinsky. Learning local equivariant representations for large-scale atomistic dynamics, 2022.

[27] Ryotaro Okabe, Abhijatmedhi Chotrattanapituk, Artittaya Boonkird, Nina Andrejevic, Xiang Fu, Tommi S. Jaakkola, Qichen Song, Thanh Nguyen, Nathan Drucker, Sai Mu, Bolin Liao, Yongqiang Cheng, and Mingda Li. Virtual node graph neural network for full phonon prediction, 2023.

[28] Cameron J. Owen, Steven B. Torrisi, Yu Xie, Simon Batzner, Jennifer Coulter, Albert Musaelian, Lixin Sun, and Boris Kozinsky. Complexity of many-body interactions in transition metals via machine-learned force fields from the tm23 data set, 2023.

[29] Bo Peng, Yuchen Hu, Shuichi Murakami, Tiantian Zhang, and Bartomeu Monserrat. Topological phonons in oxide perovskites controlled by light. *Science Advances*, 6(46), November 2020.

[30] John P. Perdew, Kieron Burke, and Matthias Ernzerhof. Generalized gradient approximation made simple. *Phys. Rev. Lett.*, 77:3865, Oct 1996.

[31] John P. Perdew, Adrienn Ruzsinszky, Gábor I. Csonka, Oleg A. Vydrov, Gustavo E. Scuseria, Lucian A. Constantin, Xiaolan Zhou, and Kieron Burke. Restoring the density-gradient expansion for exchange in solids and surfaces. *Phys. Rev. Lett.*, 100:136406, Apr 2008.

[32] Guido Petretto, Shyam Dwaraknath, Henrique P. C. Miranda, Donald Winston, Matteo Giantomassi, Michiel J. van Setten, Xavier Gonze, Kristin A. Persson, Geoffroy Hautier, and Gian-Marco Rignanese. High-throughput density-functional perturbation theory phonons for inorganic materials. *Scientific Data*, 5(1):180065, 2018.

[33] Robert M. Pick, Morrel H. Cohen, and Richard M. Martin. Microscopic theory of force constants in the adiabatic approximation. *Phys. Rev. B*, 1:910–920, Jan 1970.

[34] Ghanshyam Pilania and Turab Lookman. Electronic structure and biaxial strain in rbhgf_3 perovskite and hybrid improper ferroelectricity in (na,rb)hg2f6 and (k,rb)hg2f6 superlattices. *Phys. Rev. B*, 90:115121, Sep 2014.

[35] Albert Reuther, Jeremy Kepner, Chansup Byun, Siddharth Samsi, William Arcand, David Bestor, Bill Bergeron, Vijay Gadepally, Michael Houle, Matthew Hubbell, Michael Jones, Anna Klein, Lauren Milechin, Julia Mullen, Andrew Prout, Antonio Rosa, Charles Yee, and Peter Michaleas. Interactive supercomputing on 40,000 cores for machine learning and data analysis. In *2018 IEEE High Performance extreme Computing Conference (HPEC)*, pages 1–6. IEEE, 2018.

[36] Samuel S. Schoenholz and Ekin D. Cubuk. Jax m.d. a framework for differentiable physics. In *Advances in Neural Information Processing Systems*, volume 33. Curran Associates, Inc., 2020.

[37] Toshiro Takabatake, Koichiro Suekuni, Tsuneyoshi Nakayama, and Eiji Kaneshita. Phonon-glass electron-crystal thermoelectric clathrates: Experiments and theory. *Rev. Mod. Phys.*, 86:669–716, Jun 2014.

[38] A Togo and I Tanaka. First principles phonon calculations in materials science. *Scr. Mater.*, 108:1–5, Nov 2015.

[39] Atsushi Togo. First-principles phonon calculations with phonopy and phono3py. *J. Phys. Soc. Jpn.*, 92(1):012001, 2023.

[40] Atsushi Togo, Laurent Chaput, Terumasa Tadano, and Isao Tanaka. Implementation strategies in phonopy and phono3py. *J. Phys. Condens. Matter*, 35(35):353001, 2023.